Journal of Visualization, Vol. 11, No. 4 (2008)337-346

Regular Paper

Delta-Wing Vortex Visualization Using Micro-Sized Water Droplets Generated by an Ultrasonic Humidifier

Sohn, M. H.*[1], Lee, K. Y.*[2] and Chang, J. W.*[3]

*1 Department of Aerospace Engineering, Korea Air Force Academy, Namil-myun, Chungwon-gun, Chungbuk-Do, 363-849, Korea. E-mail: myongsohn@hanmail.net
*2 Department of Mechanical Engineering, Korea Air Force Academy, Namil-myun, Chungwon-gun, Chungbuk-Do, 363-849, Korea.
*3 Department of Aeronautical Science and Flight Operation, Korea Aerospace University, Hwajeon-dong, Deokyang-gu, Goyang-city, Gyeonggi-Do, 412-791, Korea.

Received 27 November 2007
Revised 19 May 2008

Abstract : An off-surface visualization method using micro water droplets and a laser beam sheet was developed. The average size of the water droplets generated by the home-style ultrasonic humidifier was about 5-10 μm. This method was pollution-free, eliminated the problem of toxicity, and provided a sufficient density of tracing particles for good visibility. The method was successfully applied to a visualization of the complex vortex flow of a double-delta wing with strake.

Keywords : Micro Water Droplets, Off-surface Visualization, Delta-wing, Vortex Flow.

1. Introduction

Varieties of smoke and vapor have been used as tracer particles in research requiring the visualization of air flows. To become an ideal tracer particle, it has to fulfill several requirements such as being nontoxic, neutrally buoyant, stable against mixing with the working fluid, and most importantly visible. However, it is not easy to find tracer particles which satisfy all of these requirements. Most varieties of smoke and vapor used in visualizations have densities of orders of magnitude greater than the density of air. Further, neutrally buoyant particles for air flows are scarcely available. However, the neutral buoyancy requirement becomes negligible if the size (i.e., diameter) of the tracer particle is sufficiently small because the motion of small particles in air is driven by gravity and drag according to Stokes' law. Therefore, the requirement of neutral buoyancy was solved by using liquid or gas particles of small size (i.e., to the order of μm). Merzkirch (1987) listed several tracer particles used to measure air-flow velocity, the diameters of which ranged from 1 μm to 30 μm. Next, the requirement that tracer particles be stable against mixing is not easy to satisfy. Smoke generated by combusting organic material or vaporizing hydrocarbon oils are used most frequently because they are small-sized particles and easily visible; but all smoke is toxic to some degree. In addition to this problem of toxicity, the use of smoke in a re-circulating wind tunnel also creates the problem that after a certain time of operation, the tunnel is completely filled with smoke (Kim et al., 2008). For this reason, there has been a continuous effort to use a steam as the visualization tracer.

For example, Brisplinghoff et al. (1976) and Parker and Brusse (1976) developed visualization methods using a mixture of water steam and liquid nitrogen. These methods can be used successfully

over a range of relatively low speeds and require temperature-control equipment in order to generate particles of neutral buoyancy. Next, Erickson et al. (1989) used a vapor screen method to visualize the vortex flow of a delta wing for speeds in the range of Mach number 0.4 to 1.4. Further, Bouchez and Goldstein (1975) developed a method of using dry-ice (CO_2 pellets) as tracing particles with limited success due to problems of inconvenience in lengthy and repeating experiments.

At a high angle of attack, the highly swept strake or front wing of a double-delta wing generates stable vortex pairs and produces an additional source of lift. Moreover, the strong strake vortex strengthens and stabilizes the main wing vortex, which results in improved lift-to-drag ratio performance and a delay in the vortex breakdown. Even though the strake-wing vortex interaction of a double-delta wing generally increases lift performance and stability, it can also cause unusual and nonlinear aerodynamic behavior when the angle of attack and/or sideslip angle exceeds certain limits, which results in severe departure and a buffet phenomenon. Thus finding a way to control and exploit to full advantage the development, interaction, and breakdown of the vortex flow of double-delta wings is of great worth.

The present study introduces a new method of off-surface flow visualization using micro water droplets generated by a home-style ultrasonic humidifier as the tracer particles and a laser beam sheet for illumination. The average size of the micro water droplets is about 5-10 μm. This method is pollution-free, eliminates the problem of toxicity, and provides a sufficient density of tracing particles for good visibility. The method is applied to the visualization of a complex vortex flow of a double-delta wing with strake.

2. Experimental Procedure and Techniques

2.1 Micro-sized Water Droplets Generated by an Ultrasonic Humidifier

When a piezo-ceramic oscillator is energized by an electrical current, it vibrates at a frequency of a few MHz and generates an ultrasonic wave. If this oscillator is placed below shallow water, the effect of the ultrasonic wave generates μm-sized water-droplets. These micro water droplets in turn satisfy some of the requirements of tracer particles suitable for examining the air flow mentioned earlier. They are nontoxic, small enough to negate the buoyancy effect, visible to any kind of optical device, and do not pollute the wind tunnel wall. The requirement of being neutrally buoyant is assessed below.

To simulate the fluid flow exactly during the visualization, the micro water droplets must have a small diffusion rate and sedimentation velocity. However, theses two requirements are somewhat contradictory in that an increase in droplet size causes the sedimentation velocity to increase but causes the diffusion rate to decrease. Assuming the water-droplets are spherical in shape, the sedimentation velocity can be calculated as follows. By applying Stokes' law, the sedimentation velocity V_S is given by Merzkirch (1987) as,

$$V_S = \frac{g d_P^2}{18 \nu_F} (\rho_P / \rho_F - 1) \tag{1}$$

where d_P is the diameter of the micro water droplets, ρ_P is the density of the micro water droplets (water), ρ_F is the working fluid (air) density, ν_F is the kinematic viscosity of the fluid (air), and g is the gravitational acceleration.

The sedimentation velocity in the present analysis was calculated to be 0.003 m/s based on a water-droplet size of 10 μm and by using the standard values of the flow properties of the visualization particles (water-droplets) and the working fluid (air). It should be remembered that this sedimentation velocity is the terminal velocity of the water-droplets obtained from the equilibrium of the gravity and the drag force acting on the water-droplets which are falling in the still air. The experimental observation time (Δt_{exp}) was assumed to be the time required for the visualization particles to pass the entire chord of the experimental model, and was calculated to be 0.06625 sec based on the model chord length of 0.53 m and free stream velocity of 8 m/s. The sedimentation distance of the visualization particles was then obtained by multiplying V_S and Δt_{exp}, which turned out to be about 0.2 mm at the trailing edge of the experimental model. In the actual flow condition of the present study, the water droplets would be mainly driven by local flows whose velocities were at least 1,000 times greater than the sedimentation velocity calculated above because

the core velocities of the well-organized delta-wing vortex flow were 2 or 3 times greater than the free stream velocity (8 m/sec). Therefore, the micro-sized water-droplets would follow the air flow in the vortices generated by the sharp-edged delta-wing of the present study. Even though the neutral buoyancy of the water-droplets generated by the ultrasonic humidifier was inferior to that of the smokes generated by combusting organic material or vaporizing hydrocarbon oils which have the diameter less than 1 μm, other advantages of the water-droplets of the present study such as the non-toxicity, convenience of use, and pollution-free were thought to compensate the inferiority of the neutral-buoyancy. PIV measurement was conducted and the results were compared with the visualization results, which will be described later. The traceability of the micro-sized water-droplets was also ascertained by the PIV measurement.

Figure 1 shows the experimental setup of the off-surface visualization technique. Water droplets of 5-10 μm in size were generated by a home-style ultrasonic humidifier. The water droplets exited 250 mm upstream from the model apex and flowed with the air stream without any external power. The exhaust nozzle of the humidifier and the wedge-shaped exit pipe were connected by a flexible tube. Two or more humidifiers can be used if needed by branching the flexible connecting tube.

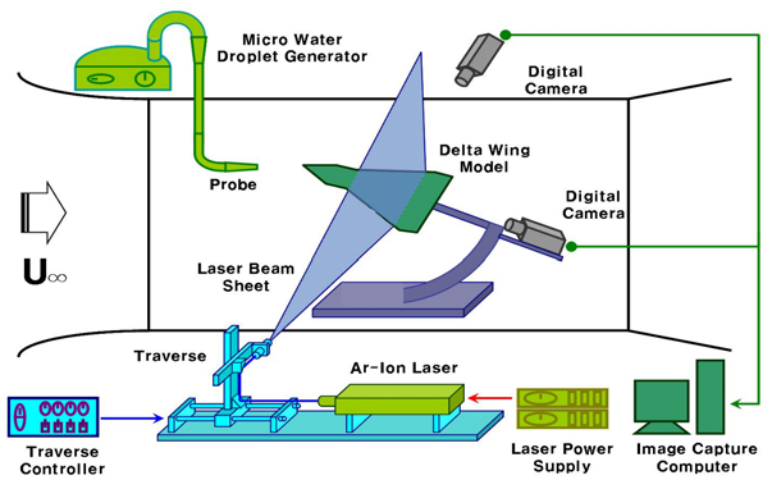

Fig. 1. Experimental setup for off-surface visualization.

2.2 Illumination and Photographic Technique

A 3W Argon ion laser was used to generate a light sheet. The laser light sheet projected by 2 cylindrical lenses and 2 convex-focusing lenses was used to interrogate specific sections of the wing-leeward flow region. It was set up perpendicular to the wing surface in order to take pictures of the cross-section. The illuminated planes were recorded at 30 frames per second by a high-resolution digital camera (SONY DCR-VX 2000 NTSC). The camera lens was positioned 470 mm behind the trailing edge of the experimental model, and the line of sight of the camera was parallel to the upper wing surface. The laser light sheet on the traverse platform was moved downstream at a constant speed while the camera took pictures at a shutter speed of 1/90 sec. For each flow condition, a total of 460-480 frames were obtained while the laser light sheet traveled from the 23 % chord position to the 100 % chord position as measured from the main-wing apex. The laser beam sheet can be set to a specific chord position while the camera takes dynamic images of the cross section of the wing-leeward flow region. Also, the laser beam sheet can be placed laterally in order to take pictures of the lengthwise cut of the wing-leeward flow region.

2.3 Tested Model-Wing and Wind Tunnel

The model was a flat wing with a 65° sweep-angle sharp leading edge. The sharp leading edge was obtained by beveling 25° on the lower surface, leaving the upper surface flat. The trailing edge was also beveled in the same way. The model had a root chord of 530 mm with the strake, the trailing

edge had a span of 317 mm, and the thickness of the wing section was 10 mm. The strake was also a 4mm-thick flat plate and had symmetrically beveled leading and side edges. The planform of the strake had sweep angles of 65° and 90°. Figure 2 shows the experimental model used. The model was supported by a rear strut attached to its trailing edge and did not have any fuselage-like structure or center-body.

The flow visualization was carried out in a low-speed wind tunnel at the Korea Air Force Academy, which had a test section size of 0.9 m high, 0.9 m wide, and 2.1 m long. The turbulence intensity was less than 0.3 % for the available test-section speed range from 3.6 m/s to 50.0 m/s, and the flow Reynolds number was 1.82×10^5 based on the freestream velocity of 8.0 m/s and the main-wing root chord of 400 mm.

In the present study, x represents the coordinate along the wing centerline measured from the main wing apex, y is the coordinate along the wing-span measured from the wing centerline, and z is the height above the upper wing surface. The wing centerline chord of 400 mm is denoted by 'c' and the local semi-span is denoted by 's'.

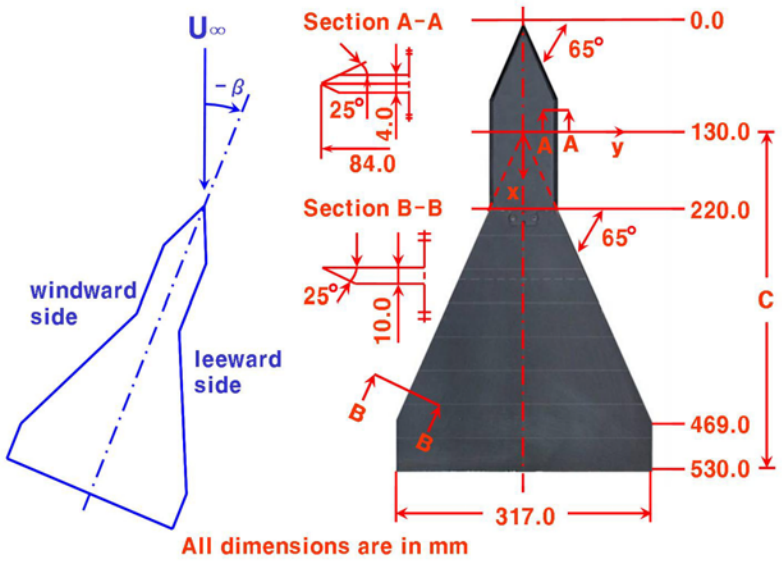

Fig. 2. Experimental model, coordinates and definition of sideslip angle (β).

3. Application and Results

3.1 Vortex Development and Interaction of Wing and Strake Vortices

Figure 3 shows a cross-sectional cut of the wing-leeward flow region above the wing-upper surface, which exhibits the chordwise development and the interaction of the wing and strake vortices of a double-delta wing configuration with strake. The angle of attack was 24° and the sideslip angle was zero. The wing-leeward flow region was dominated by a strong strake vortex pair at x/c = 0.23 (Fig. 3(a)) at a point just downstream from the junction of the strake and the main wing. At x/c = 0.30 (Fig. 3(b)), the wing vortex pair just started to develop in the vicinity of the wing leading edge, but the wing-leeward flow region was still dominated by the strake vortex pair. Going downstream, the wing vortex increased in strength and size due to the feeding of vorticity of the same sign through the shear layer which connected the wing vortex and the wing leading edge. The wing and strake vortices on both sides of the wing co-rotated and migrated in the spanwise and normal directions according to the rule of mutual induction of a vortex pair with the same sense of rotation. At x/c = 0.43 (Fig. 3(c)), the wing and strake vortices were positioned laterally at nearly the same vertical distance from the wing surface. The clockwise coiling of the wing and strake vortices on the port side of the wing as well as the counterclockwise coiling of the wing and strake vortices on the starboard side of the wing continued as the flow moved downstream. At x/c = 0.60 (Fig. 3(e)), the core of the wing vortex was

located directly above the core of the strake vortex. Thus, the wing vortex and the strake vortex each rotated about 90° while traveling from x/c = 0.43 to x/c = 0.60. The size of the wing and strake vortices were comparable after x/c = 0.60. The last frame of Fig. 3 shows that the wing and strake vortices merge to make a single vortex without breakdown at the trailing edge (x/c = 1.0). Each image in Fig. 3 is of course not a unique image of the cross-section at the specific chord position. Rather, the dynamic images of the specific section showed that wandering of the core positions of the vortices and their coiling state occurred, and that the amplitude of this wandering increased when the angle of attack or the chord position was increased. However, the deviation of the core position was within 5 %.

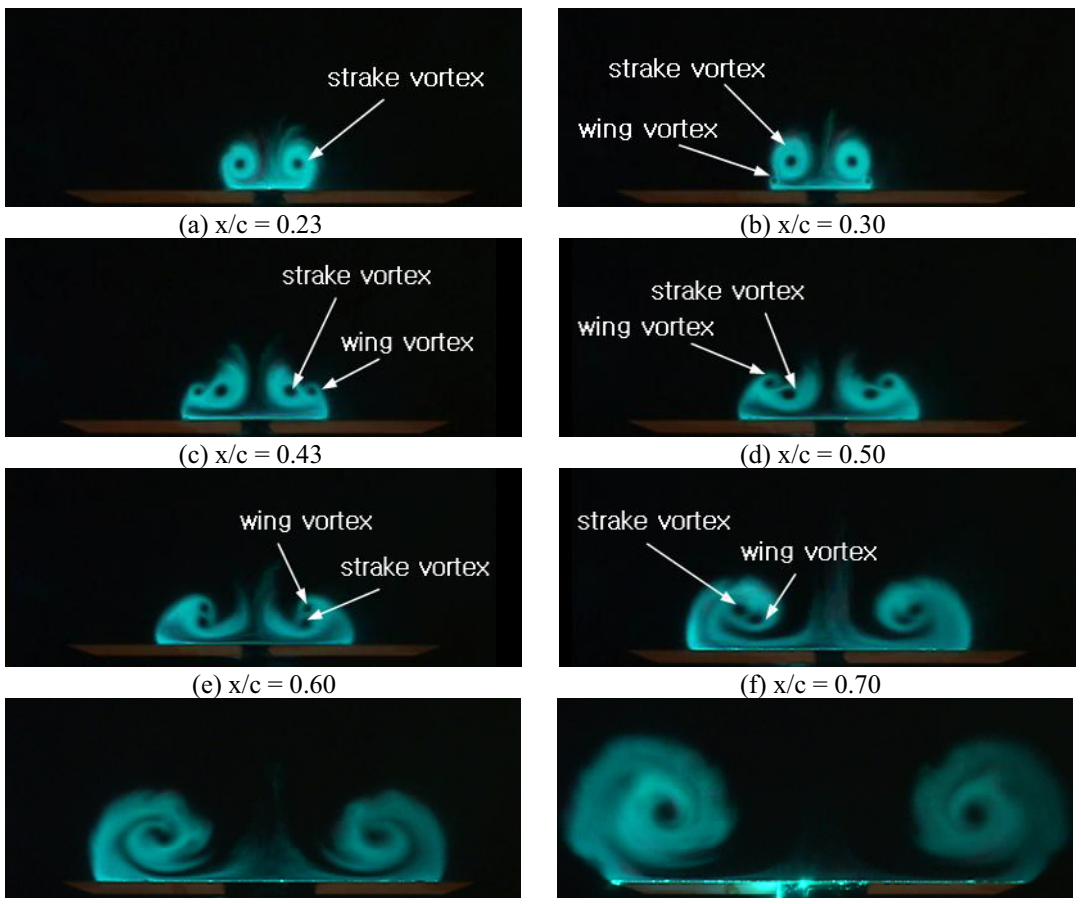

(a) x/c = 0.23 (b) x/c = 0.30

(c) x/c = 0.43 (d) x/c = 0.50

(e) x/c = 0.60 (f) x/c = 0.70

(g) x/c = 0.80 (h) x/c = 1.0

Fig. 3. Cross-sectional cut of the wing and strake vortices (α = 24° and β = 0°).

Figure 4 shows a cross-sectional cut of the wing-leeward flow region above the wing-upper surface for the case of angle of attack α = 24° and sideslip angle β = –5°. According to the definition of the sideslip angle shown in Fig. 2, the port side of the wing is the windward side and the starboard side of the wing is the leeward side at β = –5°. In this case, the sideslip caused the strake and wing vortices to move inboard and closer to the wing surface on the port side, and to move outboard and farther from the upper wing surface on the starboard side, compared to the zero sideslip case. The intertwining of the wing and stake vortices and their helical trajectory while going downstream were the same as that in the zero sideslip case. However, for the case of sideslip angle β = –5°, the clockwise coiling of the wing and strake vortices on the windward side increased slightly, and the counterclockwise coiling of the wing and strake vortices on the leeward side decreased significantly. The windward wing and strake vortices coalesced and diffused after the 70 % chord station, while the leeward wing and strake vortices floated away from the wing surface, each with distinct cores. The leeward wing and strake vortices combined to produce one vortex system at the trailing edge as shown in Fig. 4(h). In summary, the effect of sideslip was the enhancement of the coiling and merging

of the wing and strake vortices on the windward side, and the suppression of the coiling and merging of the wing and strake vortices on the leeward side.

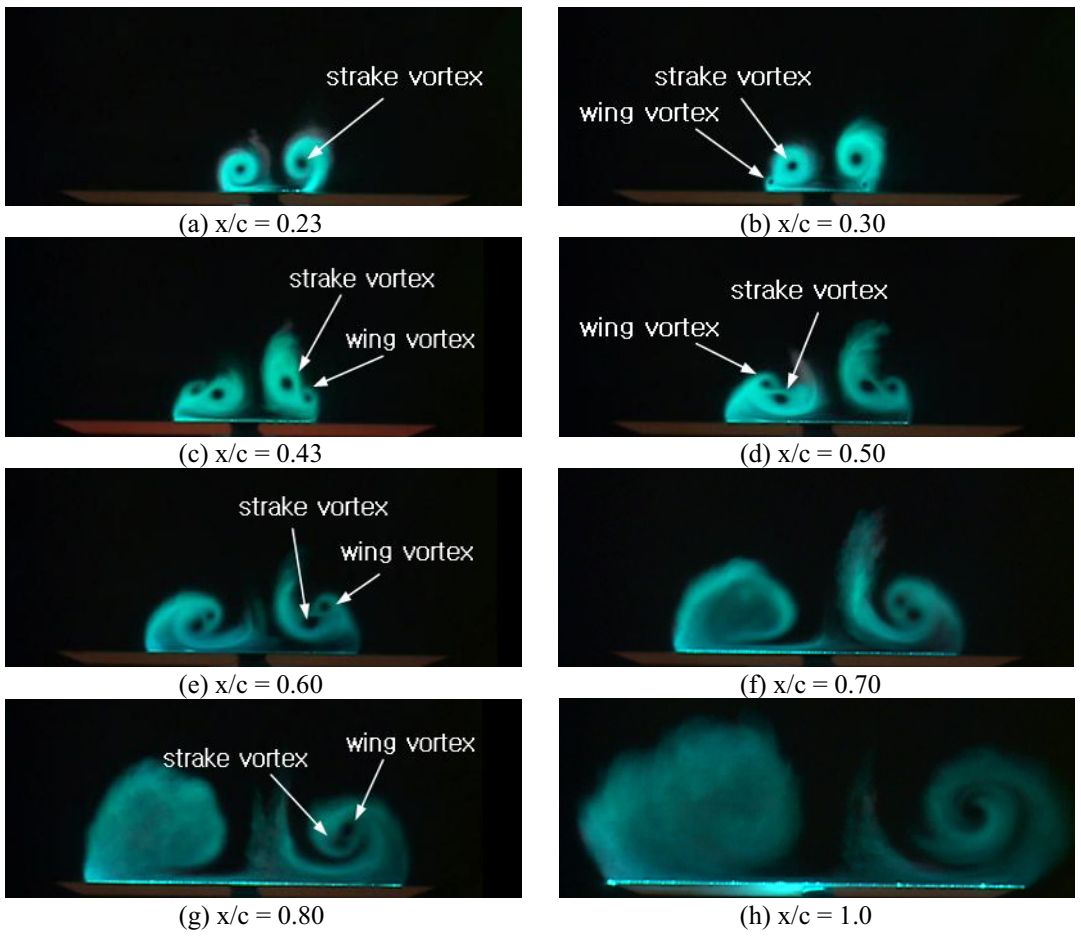

(a) x/c = 0.23 (b) x/c = 0.30

(c) x/c = 0.43 (d) x/c = 0.50

(e) x/c = 0.60 (f) x/c = 0.70

(g) x/c = 0.80 (h) x/c = 1.0

Fig. 4. Cross-sectional cut of the wing and strake vortices (α = 24° and β = -5°).

Figure 5 shows a lengthwise cut of the vortex flow viewed from the tunnel ceiling. The laser beam sheet was placed laterally so that the lengthwise cut of the vortex cores could be illuminated. The cores of the wing and strake vortices performed a helical motion as they passed the wing, as described earlier. Thus, just one slice of a laser beam sheet was not able to capture all of the vortex cores in the wing-leeward flow region above the wing-upper surface. Therefore, the inclination angle and the vertical position of the laser beam sheet were adjusted to manifest specific vortex cores for each angle of attack. The positions of the laser beam sheet and the model planform shape are schematically indicated in each frame of Fig. 5.

In Fig. 5(a), the laser beam sheet cut the wing surface at x/c = 0.33 and made a 20° angle with the wing-upper surface, making an angle of 4° with the free stream. The cores of the strake and wing vortices at the upstream chord positions were clearly captured, as shown in Fig. 5(a). The strake vortex cores were located inboard, and the wing vortex cores were located outboard. At x/c = 0.43, both the strake vortex cores and the wing vortex cores were captured, but only the wing vortex cores were captured at x/c = 0.50. This is because the strake vortex core missed the laser beam sheet due to downward migration. After x/c = 0.60 none of the vortex cores could be captured since all vortices were located below the laser beam sheet.

A more comprehensive structure of the vortex system was captured by the laser beam sheet which was parallel to the wing surface, as shown in Fig. 5(b). The cores of the strake vortex were observed over almost the entire wing region. Before x/c = 0.30 no vortex was observed since the strake and wing vortices were above and below the laser beam sheet, respectively. The trajectory of the strake vortex core was straight up to about x/c = 0.50, after which it bent outboard. It was

observed that the weaker wing vortex revolved around the stronger strake vortex at upstream chord positions, and that the wing and strake vortices of comparable strength co-rotated around each other at downstream chord positions. This different interaction between the wing and strake vortices at different chord positions determined the behavior of the core trajectory of the strake vortex described above. At x/c = 0.43 the cores of both the wing and strake vortices were observed, but the cores of the wing vortices could not be observed at x/c = 0.50 and 0.60 since the wing vortex cores migrated upward between these two chord positions. At x/c = 0.70 the wing vortex cores were observed inboard of the strake vortex cores, and the merged vortex cores were observed thereafter. Srigrarom and Lewpiriyawong (2007) investigated the behavior of the leading-edge vortex breakdown depending the wing-sweep angle and wing-surface modification with hemisphere-like bulges. They observed that the straightness of the leading-edge vortex cores became wavy as they went downstream at the angle of attack 25 degree for 60 and 65-degree sweep models. The strake and wing vortices of the present study did not show any waviness in their downstream trajectory at the angle of attack 24-degree. Instead they coiled according the rule of mutual induction as described before. The strong strake vortex of the double-delta wing configuration of the present study is thought to contribute to the stabilization of the vortex system as noted in Sohn et al. (2004).

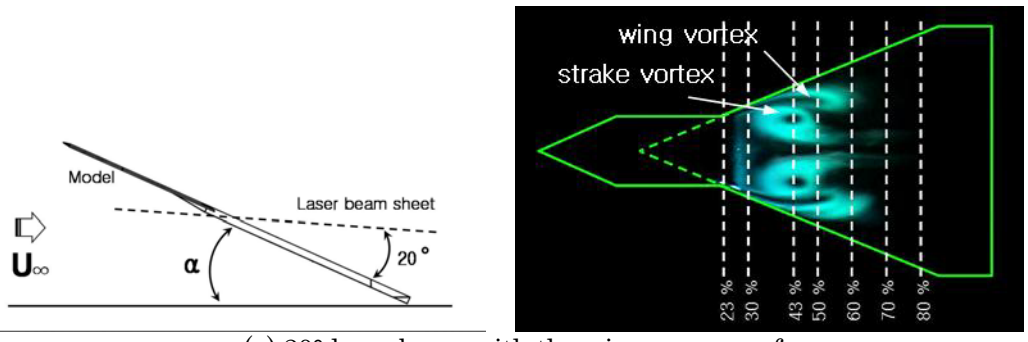

(a) 20° laser beam with the wing-upper surface

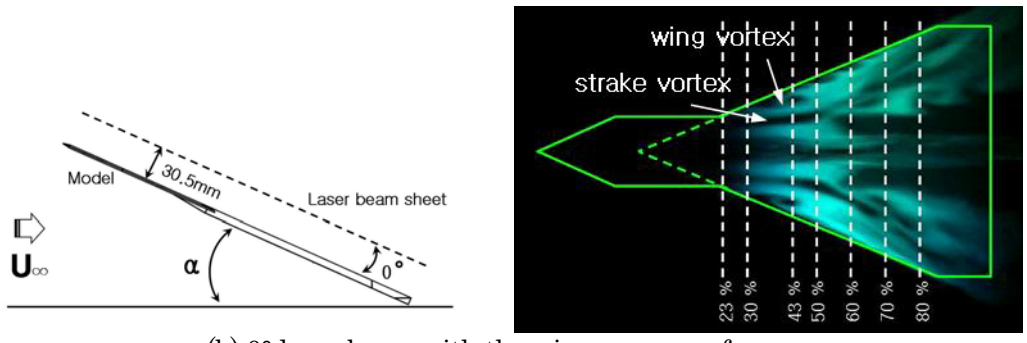

(b) 0° laser beam with the wing-upper surface

Fig. 5. Lengthwise cut of the wing and strake vortices (α = 24° and β = 0°).

3.2 Comparison with PIV Measurement

The PIV measurement of the cross-flow velocity vector in the wing-leeward flow region was conducted with a scaled model at another Korea Air Force Academy low-speed wind tunnel with PIV facilities. The medium-scale test facility was a closed-circuit atmospheric tunnel having a test section 3.5 m wide × 2.45 m high × 8.7 m long with a maximum freestream velocity of 92.0 m/s. The main wing of the model had a root chord of 600 mm, the trailing edge had a span of 475.4 mm, and the thickness of the wing section was 15.0 mm. Also, the strake was a 6.35mm-thick flat plate and had symmetrically beveled leading and side edges. PIV System used consists of a double-pulse Nd:YAG laser (Vlite-200) with a maximum pulse energy of 2 × 200 mJ at a repetition rate of 10Hz, a 8-bit digital CCD with a resolution of 2048 × 2048 pixels, and a PC equipped with DaVis FlowMaster software and a synchronization board developed by LaVision GmbH for the system synchronization, control, data acquisition and post-processing. An aerosol generator was used for DEHS ($C_{26}H_{50}O_4$)

particle seeding. The PIV data was an ensemble average of 20 instantaneous velocity fields. Details of the PIV measurement system and the uncertainty estimation are available in Sohn and Chung (2005).

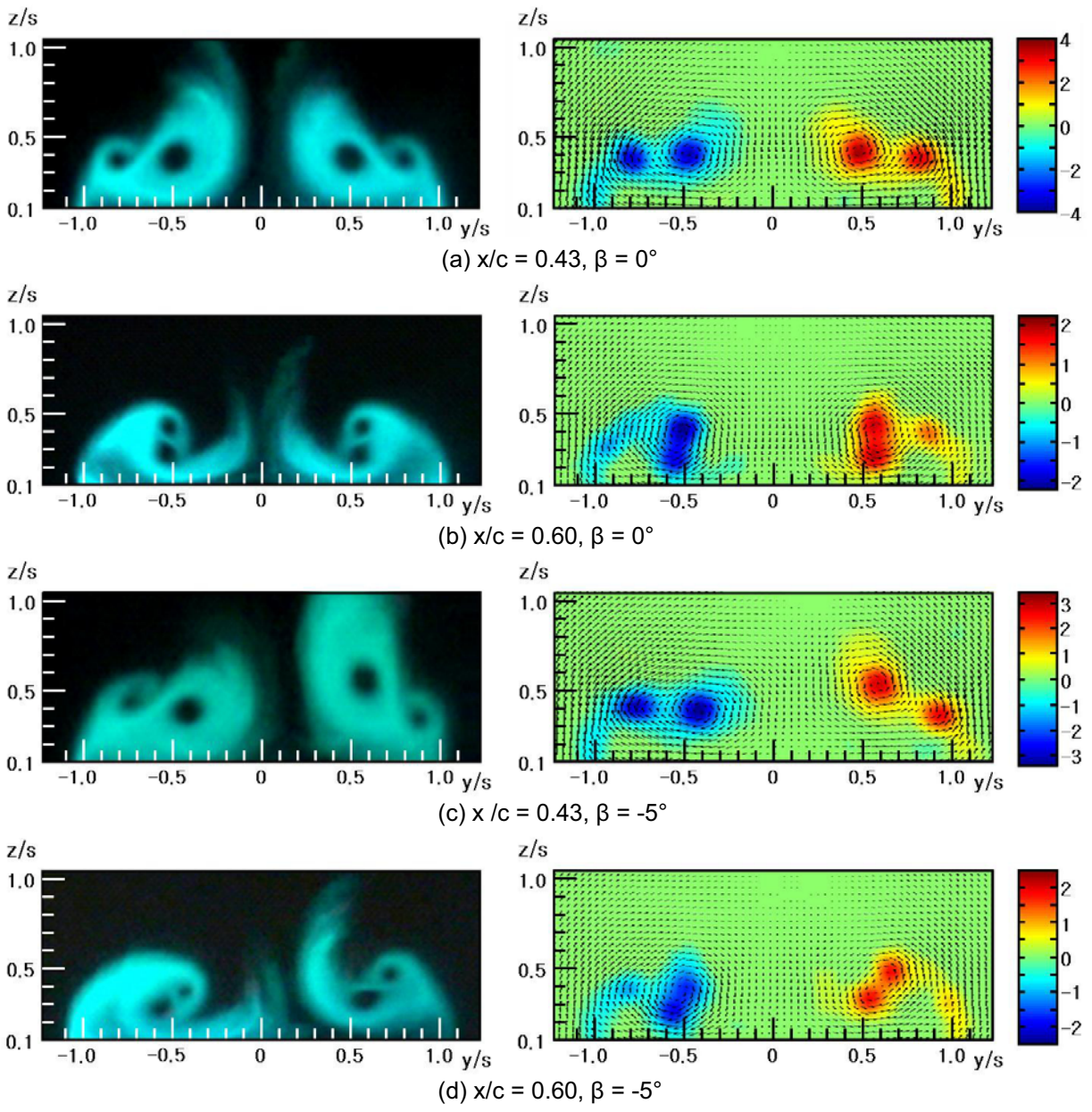

(a) x/c = 0.43, β = 0°

(b) x/c = 0.60, β = 0°

(c) x /c = 0.43, β = -5°

(d) x/c = 0.60, β = -5°

Fig. 6. Comparison of visualization and PIV measurement (α = 24°).

The visualization photos on the left-hand side of Fig. 6 show the cross-section views, while the images on the right-hand side show the cross-flow velocity vectors and the streamwise vorticity contours obtained by the PIV measurement. The streamwise vorticity was obtained by differentiating the measured cross-flow velocity field. The flow Reynolds number of the PIV measurement based on the free stream velocity (10 m/sec) and the main-wing chord (600 mm) was 4.4×10^5. In Fig. 6, the spanwise coordinate (y) and the normal coordinate (z) were normalized by the local semi-span 's'. The comparison shows a fairly good agreement between the two results regarding the relative positions of the wing and strake vortices as well as their interaction at the upstream chord position x/c = 0.43 even though the size of the models and the wind tunnels used for the visualization and the PIV measurement were different. The PIV measurement in Fig. 6 confirms

that the streaklines which connect the wing leading edge and the wing vortex core are the shear layers of vorticity feeding. At the downstream chord position x/c = 0.60, the visualization result and the PIV measurement show deviation. The flow visualization results show excellent symmetry between the port-side wing-half and the starboard-side wing half. However, the PIV measurement does not show a good symmetry between the vortex flows of the two sides of the wing. The coiling of the wing and strake vortices was delayed slightly on the starboard side of the wing compared to that on the port side of the wing, which made an asymmetric flow pattern between the two sides of the wing. This asymmetry of the flow pattern in the PIV measurement was disconcerting. The decreased resolution of the PIV measurement and/or the intrinsic flow unsteadiness might have caused the asymmetry of the flow at x/c = 0.60.

The case of non-zero sideslip angle was shown in Figs. 6(c)and (d). The effect of the sideslip is manifested both in the visualization and PIV results. The cores of the strake and wing vortices moved inboard and closer to the wing surface on the windward side, whereas they moved outboard and farther from the upper wing surface on the leeward side. PIV measurement showed that at x/c = 0.43 the wing vortex was stronger than the strake vortex on the windward side, while the wing and strake vortices had nearly the same strength on the leeward side. At x/c = 0.60 the strengths of the vortices were reduced significantly on the windward side, while the wing and strake vortices maintained their strengths and identity on the leeward side.

4. Conclusion

A new method of off-surface flow visualization using micro water droplets generated by a home-style ultrasonic humidifier as tracer particles and a laser beam sheet was developed. The average size of the micro water droplets was about 5-10 μm. The sedimentation velocity of the tracer particle was calculated to be 0.003 m/s, and the sedimentation distance was about 0.2 mm at the trailing edge of the experimental model. The present method was pollution-free, eliminated problems of toxicity, and provided enough density of tracing particles for good visibility.

The method was successfully applied in a visualization of a complex vortex flow of a double-delta wing with strake. The visualization results of the chordwise development and the interaction of the wing and strake vortices of the tested model revealed that the strake and wing vortices spiraled around each other while maintaining comparable strength and identity before they merged into a single vortex. The major effect of sideslip was enhancement of the coiling and diffusion of the wing and strake vortices on the windward side, and the suppression of the coiling and diffusion of the wing and strake vortices on the leeward side.

Acknowledgements

This research was sponsored by the Korea Science and Engineering Foundation (Grant Number KOSEF R01-2003-000-10744-0). The authors would like to thank KOSEF.

References

Bisplinghoff, R. L., Coffin, J. B. and Holdeman, C. W., Water Fog Generation System for Subsonic Flow Visualization, AIAA Journal, 14-8 (1976), 1133-1135.

Bouchez, J. P. and Goldstein, R. J., Impingement Cooling from a Circular Jet in a Cross Flow, International Journal for Heat and Mass Transfer, 18 (1975), 718-730.

Erickson, G. E., Schreiner, J. A. and Rogers, L. W., On the Structure, Interaction, and Breakdown Characteristics of Slender Wing Vortices at Subsonic, Transonic, and Supersonic Speeds, AIAA Atmospheric Flight Mechanics Conference (Boston Massachusetts, USA), AIAA Paper 1989-3345, (1989).

Kim, S. H., Chang, J. W. and Sohn, M. H., Flow Visualization and Aerodynamic-Force Measurement of a Dragonfly-Type Model, Journal of Visualization, 11-1 (2008), 37-44.

Merzkirch, W., Flow Visualization (2nd ed.), (1987), Academic Press, New York.

Parker, A. G. and Brusse, J. C., New Smoke Generation for Flow Visualization in Low Speed Wind Tunnel, Journal of Aircraft, 13-1 (1976), 57-58.

Sohn, M. H., Lee, K. Y. and Chang, J. W., Vortex Flow Visualization of a Yawed Delta Wing with Leading-Edge Extension, Journal of Aircraft, 41-2 (2004), 231-237.

Sohn, M. H. and Chung, H. S., PIV and CFD Analyses of Vortical Flow of a Yawed LEX-Delta Wing Configuration, AIAA Applied Aerodynamics Conference (Toronto Ontario, Canada), AIAA Paper 2005-4853, (2005).

Srigrarom, S. and Lewpiriyawong, N., Controlled Vortex Breakdown on Modified Delta Wing, Journal of Visualization, 10-3 (2007), 299-307.

Author Profile

Myong Hwan Sohn: He received his B.S. degree in aerospace engineering from the Korea Air Force Academy in 1977, and his M.S. and PhD degrees from Seoul National University and Georgia Institute of Technology in 1980 and 1986, respectively. He is currently a professor in the Department of Aerospace Engineering at the Korea Air Force Academy. His research interests include unsteady aerodynamics, bio-fluid mechanics, and flow control.

Ki Young Lee: He received his B.S. degree in Mechanical Engineering from the Korea Air Force Academy in 1981, and his M.S. and PhD degrees from Seoul National University and University of Utah in 1985 and 1994, respectively. He is currently a professor in the Department of Mechanical Engineering at the Korea Air Force Academy. His research interests include flow control, experimental fluid mechanics and jet propulsion engine.

Jo Won Chang: He received his B.S. degree in aerospace engineering from the Korea Air Force Academy in 1982, and his M.S. and Ph.D. degrees from Seoul National University and KAIST in 1986 and 1999, respectively. He is currently an associate professor in the Department of Aeronautical Science and Flight Operation at Korea Aerospace University in Korea. His research interests include unsteady aerodynamics, bio-fluid mechanics, wind tunnel experiments, and flight tests.